

# EEG Dipole Source Localization in Hemispherical Harmonics Domain

Amita Giri, Lalan Kumar and Tapan Gandhi  
 Indian Institute of Technology, Delhi  
 E-mail: {eez178183, lkumar, tgandhi}@ee.iitd.ac.in

**Abstract**—Dipole source localization problem is addressed in hemispherical harmonics (HSH) domain. Human head is approximated by spherical head model. Hence, spherical harmonics (SH) basis functions have been natural choice for EEG source reconstruction and localization. However, sensor placed over scalp to acquire EEG signal, assume the shape of a hemisphere. Hemispherical harmonics basis functions will more appropriately represent the data sampled over hemisphere. In this paper, the forward data model is formulated in HSH domain. Optimal array processing methods for source localization such as Multiple Signal Classification (MUSIC) and minimum variance distortionless response (MVDR) are proposed in HSH domain. Various experiments have been presented to illustrate the theory.

## I. INTRODUCTION

Dipole source localization (DSL) has been an active area of research in the recent years because of clinical and research applications [1, 2, 3]. DSL is done using electroencephalogram (EEG) or magnetoencephalogram (MEG) signals. EEG signal generation is modeled using equivalent charge, equivalent potential and equivalent current dipole. The equivalent current dipole (ECD) model is used widely as it models ion flow from one neuron (current source) to the other neuron (sink). Current source and sink constitute the current dipole in brain. The current dipole is parameterized by its magnitude, location and orientation. DSL involves estimation of these dipole parameters. The DSL problem is formulated using underdetermined and overdetermined approach, referred as dipole imaging and dipole fitting respectively. Underdetermined source models give distributed solutions all over the brain. Overdetermined approach to DSL gives compact representation of distributed sources in a clustered sense, thus can be used to represent concisely the source distribution. Various approaches to overdetermined DSL problem have been proposed that include models for one dipole [4], multiple dipoles [5], Soft computing [6], likelihood estimation with fMRI data [7, 8], PCA fitting [9], artificial neural network [10] and MUSIC [11]. All these approaches make use of spatial domain signal processing.

Spherical harmonics domain processing has received significant attention for acoustic source localization and beamforming in the recent years due to ease of array processing in SH domain with no spatial ambiguity [12, 13]. A spherical sensor array is utilized for this purpose. In literature, the human head is approximated by spherical head model [14]. Hence, spherical harmonics basis functions have been natural choice for EEG source reconstruction and localization [15, 16, 17]. Spherical harmonics were utilized in spatial

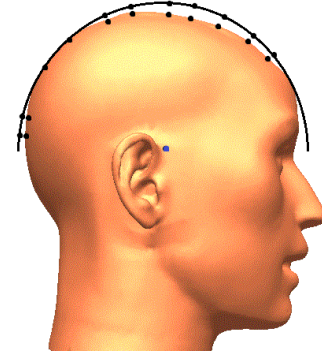


Fig. 1: Typical head model with projection of sensor positions over hemisphere.

filtering of MEG multichannel measurements to any user-specified spherical region of interest (ROI) inside the head [18]. Spherical harmonics in general, are utilized to represent function defined over entire sphere. For DSL, the EEG signal is acquired using sensors placed over scalp. Spatial sampling of EEG signal over scalp can be approximated as a hemisphere as shown in Fig. 1. Accurate representation of data over hemisphere by SH requires more number of SH coefficients due to discontinuities at the boundary of the hemisphere [19, 20]. Hence, hemispherical harmonics basis function will more appropriately represent the data sampled over hemisphere. HSH basis functions are utilized in [19] for hemispherical radiance function representation and in [20] for acoustic source localization. In this paper, overdetermined approach based on hemispherical harmonics MUSIC algorithm is explored for DSL. The novelty of work is in utilization of hemispherical harmonics domain processing for DSL.

## II. SPATIO-TEMPORAL FORWARD DATA MODEL

In this Section, spatio-temporal data model is derived using infinite homogeneous isotropic conductor (IHIC) model. The co-ordinate system utilized herein, assumes origin at the center of head.  $I$  sensors are utilized to measure the potential over head. The  $p$ th source location is denoted by  $\vec{r}_p = (r_p, \theta_p, \varphi_p)^T$  where  $r_p$  is distance from a source to the origin,  $\theta_p$  is elevation angle measured downward from positive  $z$  axis, and  $\varphi_p$  is the azimuth angle measured anticlockwise from positive  $x$  axis. Similarly, the  $i$ th sensor location is given by  $\vec{r}_i = (r_i, \theta_i, \varphi_i)^T$ . The DSL problem under consideration, utilizes ECD model where each dipole is parameterized by its position

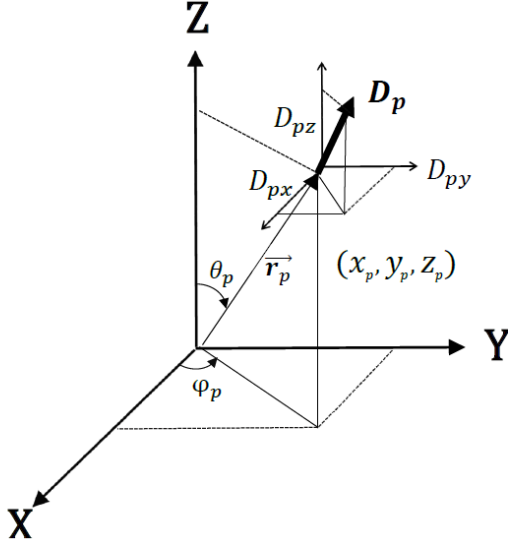


Fig. 2: The dipole parameters.

$\vec{r}_p = (x_p, y_p, z_p)^T$  and dipole moment  $\vec{D} = (D_{px} D_{py} D_{pz})^T$  as shown in Fig. 2.

In the IHIC model, the brain medium is assumed to be isotropic and homogeneous with constant conductivity  $\sigma$  to avoid the reflection effects [14]. At a given instant,  $P$  regions are considered to be active in the brain medium. The electric potential measured at a point  $\vec{r}_i$  on scalp generated by the  $p$ th active region is given by the Poisson's equation as [21]

$$V_p(\vec{r}_i, t) = \frac{1}{4\pi\sigma} \int_{S_p} \vec{J}_v(t) \cdot \frac{(\vec{r}_i - \vec{r}_{pv})}{|\vec{r}_i - \vec{r}_{pv}|^3} dv, \quad (1)$$

where the integration is over a volume  $S_p$  containing the  $v$ th dipole located at  $\vec{r}_{pv}$  position vector.  $\vec{J}_v$  is the current dipole density for a dipole at elemental volume  $dv$ . In ECD model, the dipoles in volume  $S_p$  is characterized by a equivalent current dipole moment given by  $\vec{D}_p(t) = \int_{S_p} \vec{J}_v(t) dv$ . Hence, the time varying potential at sensor location  $\vec{r}_i$  due to the  $p$ th equivalent dipole can be written as

$$V_p(\vec{r}_i, t) = \frac{\vec{D}_p(t) \cdot (\vec{r}_i - \vec{r}_p)}{4\pi\sigma |\vec{r}_i - \vec{r}_p|^3} \quad (2)$$

where  $\vec{r}_p$  is the mean dipole location vector of dipoles active in the volume  $S_p$ . For the case of dipoles with fixed location and orientation, the total potential at the  $i$ th sensor for  $P$  such dipoles is given by

$$V(\vec{r}_i, t) = \sum_{p=1}^P V_p(\vec{r}_i, t) \quad (3)$$

Utilizing (2) and (3), the spatio-temporal dipole data model for  $I$  sensors and  $N_s$  time samples, can be written in matrix form as

$$\mathbf{V}_{I \times N_s} = \mathbf{G}_{I \times 3P} \mathbf{D}_{3P \times N_s}. \quad (4)$$

where,  $\mathbf{G}$  is called lead field matrix, given by

$$\mathbf{G} = [G_1 \ G_2 \ \cdots \ G_P] \quad (5)$$

with

$$G_p = [\vec{b}_{p,1} \ \vec{b}_{p,2} \ \cdots \ \vec{b}_{p,I}]^T \quad (6)$$

$$\vec{b}_{p,i} = \frac{(\vec{r}_i - \vec{r}_p)}{4\pi\sigma |\vec{r}_i - \vec{r}_p|^3}, \quad (7)$$

and  $\mathbf{D}$  is dipole moment matrix given by

$$\mathbf{D} = [D_1 \ D_2 \ \cdots \ D_P]^T \quad (8)$$

with

$$D_p = [D_{px} \ D_{py} \ D_{pz}]^T \quad (9)$$

It is to note that  $\vec{b}_{p,i}$  is  $1 \times 3$  vector and each of  $D_{px}$ ,  $D_{py}$ ,  $D_{pz}$  is  $1 \times N_s$  dipole moment time series vectors in  $X$ ,  $Y$ ,  $Z$  directions. Under fixed dipole assumption, the dipole moment matrix in (4), can further be decomposed as

$$\mathbf{D}_{3P \times N_s} = \mathbf{M}_{3P \times P} \mathbf{S}_{P \times N_s} \quad (10)$$

where  $\mathbf{M}$  represents unit orientation moments and  $\mathbf{S}$  moment intensity matrix. Substituting this in (4), the final spatio-temporal data model can be written as

$$\mathbf{V}_{I \times N_s} = \mathbf{A}_{I \times P} \mathbf{S}_{P \times N_s} \quad (11)$$

where

$$\mathbf{A}_{I \times P} = \mathbf{G}_{I \times 3P} \mathbf{M}_{3P \times P}. \quad (12)$$

The resultant data model separates time invariant (location and orientation) and time variant portions (intensity) parameters of the dipole. Which facilitate the application of subspace based methods for source localization.

### III. HEMISPHERICAL HARMONICS DOMAIN DATA MODEL

The spatio-temporal data model in (11) is reformulated herein in hemispherical harmonics domain. The hemispherical harmonics domain processing is computationally more efficient due to dimensionality reduction. In the ensuing Section, spherical harmonics decomposition of the measured potential is introduced first.

#### A. Real Spherical Harmonics Transform

Dipole source localization is performed using discrete time domain EEG. As the EEG potential signals (3) are real, we introduce the real spherical harmonics transform (SHT) defined on the sphere first. The real SHT of discrete time potential measured over scalp  $\in (R, \Omega)$  is given by

$$V_{nm}(t) = \int_{\Omega \in S^2} V(t, \Omega) [Y_n^m(\Omega)] d\Omega, \quad (13)$$

where  $Y_n^m(\Omega)$  is real valued spherical harmonics [22] of order  $n$  and degree  $m$ , defined as

$$Y_n^m(\theta, \phi) = \begin{cases} (-1)^{|m|} \sqrt{2} K_n^m \sin(|m|\phi) P_n^{|m|}(\cos \theta) & : m < 0 \\ (-1)^{|m|} \sqrt{2} K_n^m \cos(m\phi) P_n^{|m|}(\cos \theta) & : m > 0 \\ K_n^0 P_n^0(\cos \theta) & : m = 0 \end{cases} \quad (14)$$

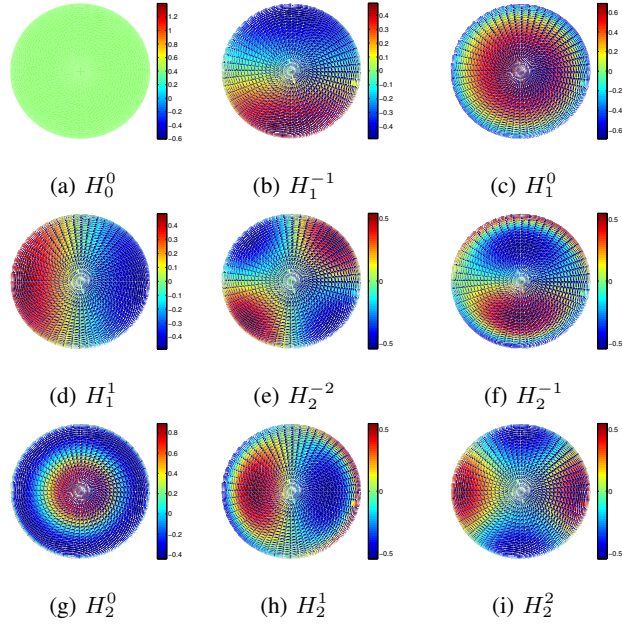


Fig. 3: Hemispherical harmonics basis upto order 2, (a)  $n = 0$ , (b) (c) (d)  $n = 1$ , (e) (f) (g) (h) (i)  $n = 2$ .

where  $P_n^m(\cos \theta)$  is the Associated Legendre Polynomial (ALPs). Replacing  $\cos \theta$  by  $x$  for simplicity, the ALPs are given as

$$P_n^m(x) = \begin{cases} (-1)^m (1-x^2)^{m/2} \frac{d^m}{dx^m} P_n(x) & : m \geq 0 \\ (-1)^m \frac{(n-m)!}{(n+m)!} P_n^{|m|}(x) & : m < 0 \end{cases} \quad (15)$$

where  $P_n(x)$  is unassociated Legendre polynomials expressed as

$$P_n(x) = \frac{1}{2^n n!} \frac{d^n}{dx^n} (x^2 - 1)^n. \quad (16)$$

The order  $n$  takes value from  $[0, \infty)$  while  $m$  varies from  $[-n, n]$ ,  $|\cdot|$  denotes the absolute value of  $(\cdot)$ ,  $K_n^m$  is the normalization value given by

$$K_n^m = \sqrt{\frac{(2n+1)(n-|m|)!}{4\pi(n+|m|)!}}. \quad (17)$$

The associated Legendre polynomials for different order  $n$  and same degree  $m$  are orthogonal over  $[-1, 1]$  with weighting function as 1 [19]. The orthogonality relation is given by

$$\int_{-1}^1 P_n^m(x) P_{n'}^m(x) dx = \frac{2(n+m)!}{(2n+1)(n-m)!} \delta_{nn'}. \quad (18)$$

The inverse real SHT is given by

$$V(t, \Omega) = \sum_{n=0}^{\infty} \sum_{m=-n}^n V_{nm}(t) Y_n^m(\Omega) \quad (19)$$

### B. Hemispherical Harmonic Decomposition of EEG Signal

The orthogonality of  $P_n^m(x)$  is over  $[-1, 1]$  as indicated in (18). The range  $[-1, 1]$  is due to the fact that the elevation angle  $\theta$ , in  $P_n^m(\cos \theta)$  takes value in  $[0, \pi]$ . As, the EEG measurement is available over hemispherical scalp, the elevation of the sensor must lie in  $[0, \pi/2]$  or equivalently,  $x \in [0, 1]$ . Hence, a new set of orthogonal associated Legendre polynomials is required. This is achieved by shifting the associated legendre polynomials. In general, if the polynomials  $P_{nm}(x)$  are orthogonal over  $[a, b]$ , with  $w(x)$  as a weighting function, then the polynomials  $P_{nm}(q_1 x + q_2)$  where  $q_1 \neq 0$  are orthogonal over an interval  $[\frac{a-q_2}{q_1}, \frac{b-q_2}{q_1}]$  with  $w(q_1 x + q_2)$  as a weighting function [23]. The linear transformation of  $x$  to  $2x - 1$  in (18) gives the shifted ALPs expressed as

$$\widetilde{P}_n^m(x) = P_n^m(2x - 1) \quad (20)$$

The shifted ALPs are orthogonal over  $[0, 1]$  with weight function as 1. The orthogonal relation is now expressed as

$$\begin{aligned} \int_0^1 \widetilde{P}_n^m(x) \widetilde{P}_{n'}^m(x) dx &= \int_0^1 P_n^m(2x - 1) P_{n'}^m(2x - 1) dx \\ &= \frac{(n+m)!}{(2n+1)(n-m)!} \delta_{nn'}. \end{aligned} \quad (21)$$

Just as ALPs are used to construct SH basis functions, shifted ALPs are utilized herein to construct a HSH basis functions orthogonal over  $[0, \frac{\pi}{2}] \times [0, 2\pi]$ . The real valued hemispherical harmonics basis functions  $H_n^m(\theta, \phi)$  can now be expressed as:

$$H_n^m(\theta, \phi) = \begin{cases} (-1)^{|m|} \sqrt{2} \tilde{K}_n^m \sin(|m|\phi) \tilde{P}_n^{|m|}(\cos \theta) & : m < 0 \\ (-1)^{|m|} \sqrt{2} \tilde{K}_n^m \cos(m\phi) \tilde{P}_n^{|m|}(\cos \theta) & : m > 0 \\ \tilde{K}_n^0 \tilde{P}_n^0(\cos \theta) & : m = 0 \end{cases} \quad (22)$$

where  $\tilde{K}_n^m$  is the normalization value expressed as

$$\tilde{K}_n^m = \sqrt{\frac{(2n+1)(n-|m|)!}{2\pi(n+|m|)!}}. \quad (23)$$

2D plots of HSH basis functions upto second order are shown in Fig. 3. Basis function values are plotted for azimuth  $[0, 2\pi]$  and elevation  $[0, \frac{\pi}{2}]$ . The above convention to represent HSH basis function is chosen to imitate the EEG scalp plots.

Utilizing (13) and (22), the hemispherical harmonics decomposition of the signal  $V(t)$  can now be expressed as

$$\begin{aligned} V_{nm}(t) &= \int_{\Omega \in S^2} V(t, \Omega) [H_n^m(\Omega)] d\Omega, \\ &\cong \sum_{i=1}^I a_i V_i(t, \Omega_i) [H_n^m(\Omega_i)], \end{aligned} \quad (24)$$

where  $a_i$  is sampling weight [24] and  $\Omega_i = (\theta_i, \phi_i)$  is the location of the  $i$ th sensor. For finite order  $n \in [0, N]$  where  $N \leq \sqrt{I} - 1$  [25] and  $m \in [-n, n]$ , (24) can be re-written in a matrix form as

$$\mathbf{V}_{\mathbf{nm}}(t) = \mathbf{H}^T(\Omega) \Gamma \mathbf{V}(t, \Omega) \quad (25)$$

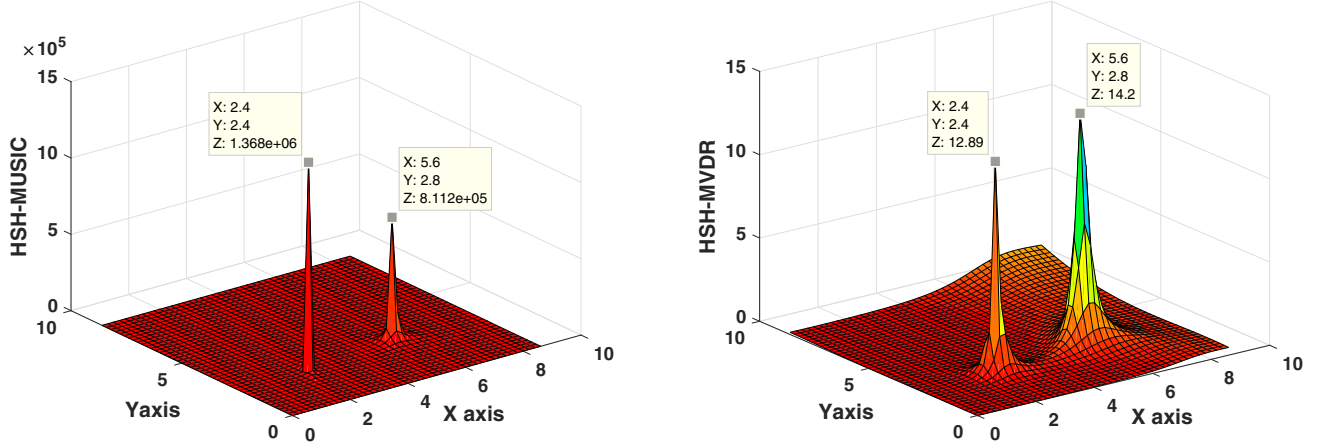


Fig. 4: Dipole source localization using HSH-MUSIC and HSH-MVDR for sources placed at  $(5.6\text{cm}, 2.8\text{cm})$  and  $(2.4\text{cm}, 2.4\text{cm})$  with 30 dB SNR.

where

$$\mathbf{V}_{\text{nm}}(t) = [V_{00}, V_{1(-1)}, V_{1(0)}, V_{1(1)}, \dots, V_{NN}]^T \quad (26)$$

$$\mathbf{\Gamma} = \text{diag} \{a_1, a_2, a_3, \dots, a_I\} \quad (27)$$

and  $\mathbf{H}(\Omega)$  is a  $I \times (N+1)^2$  matrix, whose  $i$ th row is defined as

$$h(\Phi_i) = [H_0^0(\Omega_i), H_1^{-1}(\Omega_i), H_1^0(\Omega_i), \dots, H_N^N(\Omega_i)]. \quad (28)$$

In the presence of additive sensor noise, the spatio-temporal data model in (11), can be re-written as

$$[\mathbf{V}]_{I \times N_s} = [\mathbf{A}]_{I \times P} [\mathbf{S}]_{P \times N_s} + [\mathbf{Z}]_{I \times N_s} \quad (29)$$

Multiplying both side of equation with  $\mathbf{H}^T \mathbf{\Gamma}$  and utilizing (25), the final hemispherical harmonics domain data model is written as

$$[\mathbf{V}_{\text{nm}}]_{(N+1)^2 \times N_s} = [\mathbf{A}_{\text{nm}}]_{(N+1)^2 \times P} [\mathbf{S}]_{P \times N_s} + [\mathbf{Z}_{\text{nm}}]_{(N+1)^2 \times N_s}, \quad (30)$$

where  $A_{nm} = \mathbf{H}^T \mathbf{\Gamma} \mathbf{G} \mathbf{M}$ . It is to note that the dimensionality of data model reduces from  $I$  to  $(N+1)^2$ , leading to computationally efficient approach.

#### IV. THE DIPOLE SOURCE LOCALIZATION

The hemispherical harmonics domain data model is utilized herein for source localization. In particular subspace based MUSIC method and beamforming based MVDR method are proposed. The HSH domain MUSIC expression for dipole source localization under fixed dipole assumption can now be written as

$$J_{\text{HSH-MUSIC}}(r) = \frac{1}{\mathbf{A}_{nm}^T \mathbf{P}_A^\perp \mathbf{A}_{nm}} \quad (31)$$

where  $\mathbf{P}_A^\perp = \mathbf{U}_{I-P} \mathbf{U}_{I-P}^T$ ,  $\mathbf{U}_{I-P}$  is the set of  $(I-P)$  noise eigen vectors obtained from eigen value decomposition of covariance matrix  $\mathbf{R} = E[\mathbf{V}_{\text{nm}} \mathbf{V}_{\text{nm}}^T]$ . Here,  $\mathbf{G}$  is look-up lead-field vector defined as in (6) and orientation moments  $\mathbf{M}$  is assumed to be fixed for fixed dipole assumption. The location of the dipole is estimated from the peak in the HSH-MUSIC spectrum due to orthogonality between signal and noise subspace.

The HSH MVDR can also be defined in the similar form as

$$J_{\text{HSH-MVDR}}(r) = \frac{1}{\mathbf{A}_{nm}^T \mathbf{R}^{-1} \mathbf{A}_{nm}} \quad (32)$$

The HSH-MVDR spectrum results in a peak when array steering location matches with source location.

Fig. 4 illustrates the HSH-MUSIC and HSH-MDR spectra for two dipole sources located at  $(5.6\text{cm}, 2.8\text{cm}, 2\text{cm})$  and  $(2.4\text{cm}, 2.4\text{cm}, 2\text{cm})$ . Uniform spatial sampling was taken with 37 sensors at SNR = 30 dB. Two peaks can be observed corresponding to two sources in both the spectra.

#### V. PERFORMANCE EVALUATION

Infinite homogeneous isotropic conductor head model with radius of 86 mm was considered for the simulation. Sensors were placed over hemispherical scalp at the locations shown in Fig. 5. Total 37 electrodes were placed over the scalp. For HSH MUSIC and HSH MVDR algorithm, inter-grid gap was chosen to be 2 mm. Potential data was generated using forward data model considering two point dipole source. Number of snapshot was taken to be 100. The sensor noise was taken to be additive Gaussian in nature. The performance of the proposed methods has been presented herein using computation time. HSH-MUSIC method is additionally, explored in terms of localization accuracy with variation in depth of the dipole.

A. Computation Time

For hemispherical harmonics of order  $N = 4$  the dimensionality of the data model is reduced from 37 in spatial domain to 25 in HSH domain. The effect is observed in computation time. System with Intel®Core™i7 processor, RAM 16 GB, system type 64-bit and clock speed 3.40 GHz was utilized for the evaluation. Computation time observed for the four algorithms are shown in Fig. 6. Bar plot with mean and standard deviation of computation time is plotted for 50 iterations. HSH-MUSIC method requires less computation time when compared to conventional MUSIC, conventional MVDR and HSH-MVDR method.

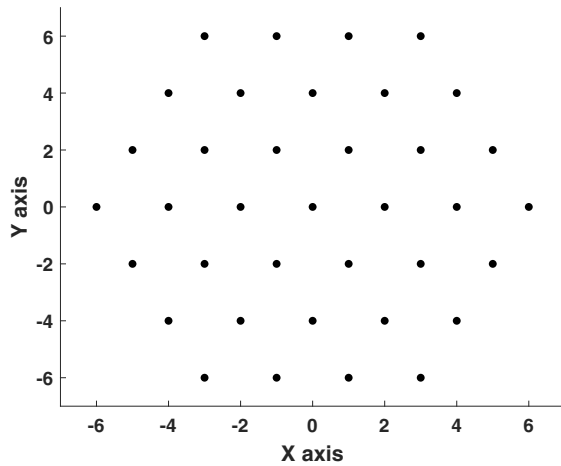


Fig. 5: Spatial sensor placement over hemispherical scalp.

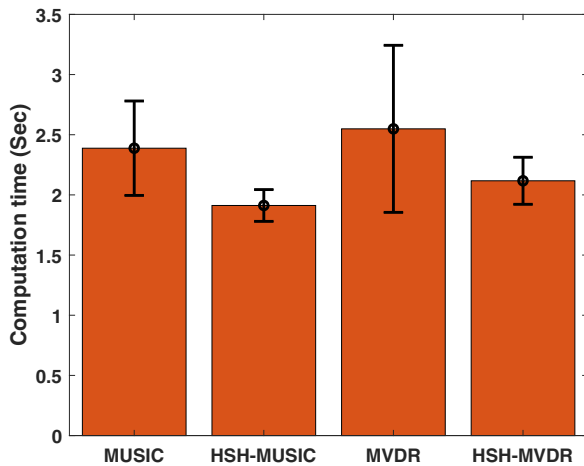


Fig. 6: Computation time.

B. Localization Accuracy with Depth Variation

Performance of the proposed algorithm is illustrated herein with variation in depth. The depth of the dipole with co-ordinate  $(x, y, z)^T$  is computed as  $\sqrt{x^2 + y^2 + z^2}$ . Two

active dipole sources were considered at depth 3.832cm with co-ordinate  $(1.3, 3, 2)^T, (3.198, 0.676, 2)^T$ . Another set of dipole sources were taken at depth 5cm with co-ordinates as  $(3.24, 3.24, 2)^T, (4.558, 0.4821, 2)^T$ . The simulation was performed considering 30dB SNR. Subspace based method being more accurate, HSH-MUSIC spectrum is plotted herein. Fig. 7 illustrates the effect of depth on the HSH-MUSIC spectrum. It is seen that the resolution of the method reduces at the higher depth.

VI. CONCLUSIONS AND FUTURE WORK

Dipole source localization in hemispherical harmonics domain is addressed for the first time in this paper. Rather than conventional spherical harmonics, hemispherical harmonics basis functions are utilized for DSL. In particular, HSH-MUSIC and HSH-MVDR are proposed for DSL. It is seen that HSH domain processing is computationally more efficient when compared to spatial domain processing. Localization and tracking of dipoles in HSH domain is currently being studied.

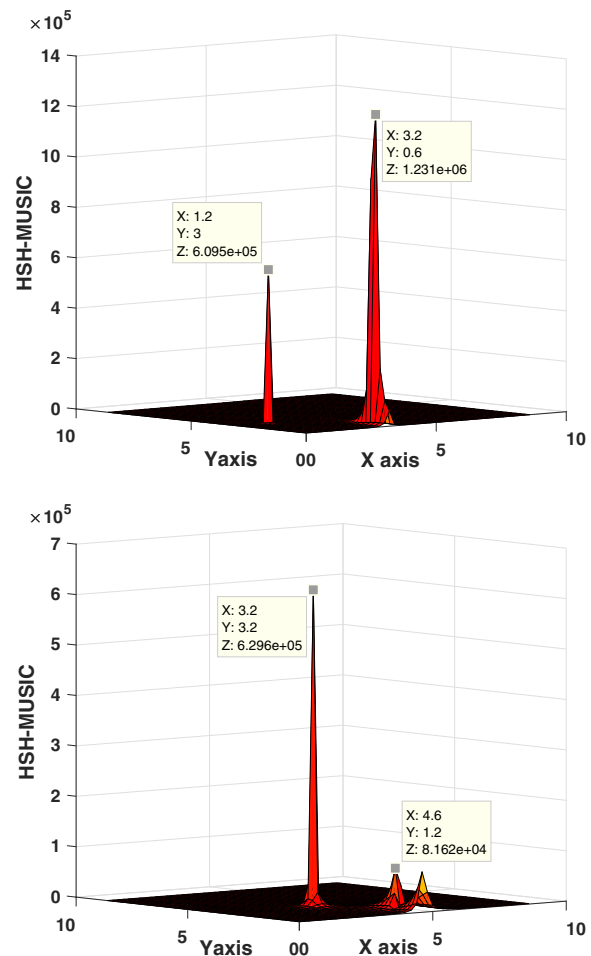


Fig. 7: HSH MUSIC cost function with depth varied as 3.8cm (above) and 5cm (below).

## ACKNOWLEDGMENT

This work was funded by Prime Minister's Research Fellowship (PMRF), Government of India.

## REFERENCES

- [1] C. Lee, R. Oostenveld, S. H. Lee, L. H. Kim, H. Sung, and J. H. Choi, "Dipole source localization of mouse electroencephalogram using the fieldtrip toolbox," *PLoS one*, vol. 8, no. 11, p. e79442, 2013.
- [2] M. Sercheli, E. Bilevicius, A. Alessio, H. Ozelo, F. Pereira, J. Rondina, F. Cendes, and R. Covolan, "EEG spike source localization before and after surgery for temporal lobe epilepsy: a BOLD EEG-fMRI and independent component analysis study," *Brazilian Journal of Medical and Biological Research*, vol. 42, no. 6, pp. 582–587, 2009.
- [3] X. Bai and B. He, "On the estimation of the number of dipole sources in EEG source localization," *Clinical neurophysiology*, vol. 116, no. 9, pp. 2037–2043, 2005.
- [4] R. G. de Peralta Menendez and S. L. G. Andino, "Single dipole localization: Some numerical aspects and a practical rejection criterion for the fitted parameters," *Brain topography*, vol. 6, no. 4, pp. 277–282, 1994.
- [5] M. Scherg, T. Bast, and P. Berg, "Multiple source analysis of interictal spikes: goals, requirements, and clinical value," *Journal of Clinical Neurophysiology*, vol. 16, no. 3, pp. 214–224, 1999.
- [6] K. Uutela, M. Hamalainen, and R. Salmelin, "Global optimization in the localization of neuromagnetic sources," *IEEE Transactions on Biomedical Engineering*, vol. 45, no. 6, pp. 716–723, 1998.
- [7] S. Ahlfors, G. Simpson, A. Dale, J. Belliveau, A. K. Liu, A. Korvenoja, J. Virtanen, M. Huutilainen, R. Tootell, H. J. Aronen *et al.*, "Spatiotemporal activity of a cortical network for processing visual motion revealed by MEG and fMRI," *Journal of Neurophysiology*, vol. 82, no. 5, pp. 2545–2555, 1999.
- [8] A. K. Liu, J. W. Belliveau, and A. M. Dale, "Spatiotemporal imaging of human brain activity using functional MRI constrained magnetoencephalography data: Monte carlo simulations," *Proceedings of the National Academy of Sciences*, vol. 95, no. 15, pp. 8945–8950, 1998.
- [9] A. Achim, F. Richer, and J. Saint-Hilaire, "Methods for separating temporally overlapping sources of neuroelectric data," *Brain topography*, vol. 1, no. 1, pp. 22–28, 1988.
- [10] G. Van Hoey, B. Vanrumste, R. Van de Walle, P. Boon, I. Lemahieu, M. D'Have, and K. Vonck, "Detection and localization of epileptic brain activity using an artificial neural network for dipole source analysis," in *Signal Processing Conference, 2000 10th European*. IEEE, 2000, pp. 1–4.
- [11] J. C. Mosher, P. S. Lewis, and R. M. Leahy, "Multiple dipole modeling and localization from spatio-temporal MEG data," *IEEE Transactions on Biomedical Engineering*, vol. 39, no. 6, pp. 541–557, 1992.
- [12] L. Kumar and R. M. Hegde, "Near-field acoustic source localization and beamforming in spherical harmonics domain," *IEEE Transactions on Signal Processing*, vol. 64, no. 13, pp. 3351–3361, 2016.
- [13] D. Khaykin and B. Rafaely, "Acoustic analysis by spherical microphone array processing of room impulse responses," *The Journal of the Acoustical Society of America*, vol. 132, no. 1, pp. 261–270, 2012.
- [14] H. Hallez, B. Vanrumste, R. Grech, J. Muscat, W. De Clercq, A. Vergult, Y. D'Asseler, K. P. Camilleri, S. G. Fabri, S. Van Huffel *et al.*, "Review on solving the forward problem in EEG source analysis," *Journal of neuroengineering and rehabilitation*, vol. 4, no. 1, p. 46, 2007.
- [15] Y. Petrov, "Harmony: EEG/MEG linear inverse source reconstruction in the anatomical basis of spherical harmonics," *PLoS one*, vol. 7, no. 10, p. e44439, 2012.
- [16] J. C. d. M. D. van 't Ent and A. L. Kaas, "A fast method to derive realistic bem models for e/meg source reconstruction," *IEEE Transactions on Biomedical Engineering*, vol. 48, no. 12, pp. 1434–1443, Dec 2001.
- [17] Dezhong and Yao, "High-resolution eeg mappings: a spherical harmonic spectra theory and simulation results," *Clinical Neurophysiology*, vol. 111, pp. 81 – 92.
- [18] T. E. Ozkurt, M. Sun, W. Jia, and R. J. Scwabassi, "Spatial filtering of MEG signals for user-specified spherical regions," *IEEE Transactions on Biomedical Engineering*, vol. 56, no. 10, pp. 2429–2438, 2009.
- [19] P. Gautron, J. Krivanek, S. N. Pattanaik, and K. Bouatouch, "A novel hemispherical basis for accurate and efficient rendering," *Rendering Techniques*, vol. 2004, pp. 321–330, 2004.
- [20] D. Kumari and L. Kumar, "Acoustic source localization in hemispherical harmonics domain," in *Proc. EuroNoise*, pp. 2575–2580, 27-31 may 2018, Crete, Greece.
- [21] J. Sarvas, "Basic mathematical and electromagnetic concepts of the biomagnetic inverse problem," *Physics in medicine and biology*, vol. 32, no. 1, p. 11, 1987.
- [22] E. T. Whittaker and G. N. Watson, *A course of modern analysis*. Cambridge university press, 1996.
- [23] G. Szeg, "Orthogonal polynomials," 4 ed. American Mathematical Society, Providence, Rhode Island, USA, 1975.
- [24] B. Raefele, "Analysis and design of spherical microphone arrays," *IEEE Transactions on Speech and Audio Processing*, vol. 13, no. 1, pp. 135–143, Jan 2005.
- [25] J. Meyer and G. Elko, "A highly scalable spherical microphone array based on an orthonormal decomposition of the soundfield," vol. 2, pp. II-1781–II-1784, May 2002.